

J. H. Nie
B. F. Armaly*

Department of Mechanical and Aerospace
Engineering,
and Engineering Mechanics
University of Missouri—Rolla,
Rolla, MO 65409

W. Q. Tao
Q. W. Wang

School of Energy and Power Engineering
Xi'an Jiaotong University,
Xi'an 710049, China

Three-Dimensional Turbulent Flow in the Exit Head Section of a Heat Exchanger

Measurements of three-dimensional turbulent flow in the exit head section of a shell-and-tube heat exchanger were performed using three-component laser Doppler velocimeter. The test geometry is half of a hemispherical cap with two outlet-tubes and with a cylindrical inlet section. Distributions of the velocity vector field, the three mean velocity components, and the Reynolds stress components are reported, and the complex nature of flow in the head section and in the neighborhood of the outlet-tube is quantified. The radial and the streamwise velocity components are of the same order of magnitude in the neighboring region of the outlet-tubes, and they are not symmetric relative to the center plane intersection of the outlet-tubes. The friction factor that was measured across the exit head section of the heat exchanger decreases as the Reynolds number increases from 25,000 to 50,000. These results are useful for validating turbulent flow simulation codes and are needed for improving the design of the exit head section of shell-and-tube heat exchangers. [DOI: 10.1115/1.1637635]

Introduction

More than 90% of the heat exchangers that are used in industry (petroleum, chemical, power generation, and heating/air-conditioning engineering) are of the shell-and-tube type design [1]. In such a system, one fluid flows inside the tubes that are encased in a shell, and another fluid flows through the shell and around the tubes. The shell is normally cylindrical in shape and has a hemispherical cap at one end. In the head section, a baffle is normally placed at the center of the hemispherical cap to separate the inlet flow to the tubes that are in the shell from the outlet flow from the tubes as it leaves the shell. In this manner, one half of the hemispherical cap serves as the inlet head section and the other half serves as the exit head section of the heat exchanger. Inlet-tubes are connected to the inlet head section, and outlet-tubes are connected to the exit head section for bringing in and for taking out the fluid that flows through the heat exchangers. The flow characteristics in the inlet head section influence the velocity distribution inside the heat exchanging tubes that are in the shell of the heat exchanger and the flow characteristics in the exit head section influence the velocity distribution in the outlet-tubes that are connected to the exit head section of the heat exchanger. Detailed knowledge of the flow distribution within the heat exchanger and in its head sections helps in the design of reliable and efficient units.

Numerous guidelines and procedures have been published [2–4] for designing and for determining the overall performance of shell-and-tube heat exchangers. In addition, few experimental [5–7] and numerical [8,9] studies have been reported on the overall flow characteristics, heat transfer and fouling performance of these heat exchangers. Unfortunately, most of the reported experimental studies have focused on the overall performance of the heat exchanger and did not report the dynamics of the internal flow and its distribution. Such data and information are needed for the optimization and the design improvements of heat exchangers. In addition, detailed flow measurements inside these heat exchangers are needed for validating simulation codes [10], and the lack of such data motivated the present study.

*Corresponding author.

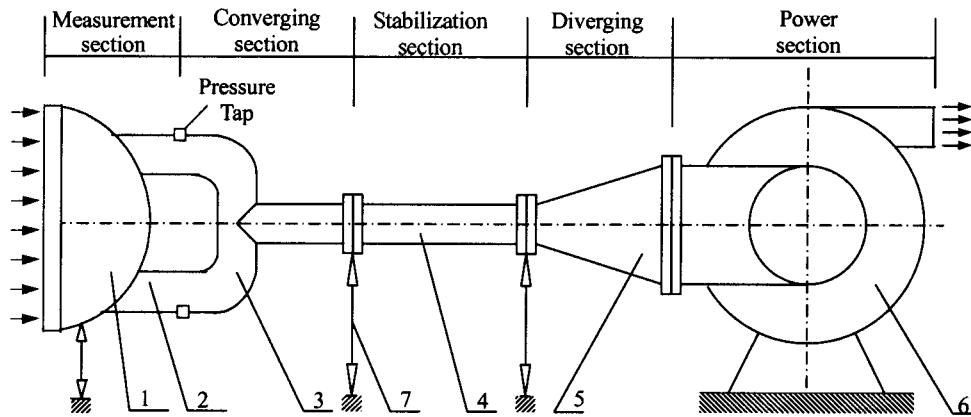
Contributed by the Fluids Engineering Division for publication in the JOURNAL OF FLUIDS ENGINEERING. Manuscript received by the Fluids Engineering Division September 11, 2001; revised manuscript received September 12, 2003. Associate Editor: J. Katz.

Experimental Apparatus and Test Sections

A schematic of the wind tunnel and the test section is shown in Fig. 1. It is an air tunnel that is composed of five sections: the measurement section, the converging section, the stabilization section, the diverging section, and the power section. The inlet section of the tunnel serves as the test section where velocity measurements are made (section 1), and it is a simplified physical model (half of a hemisphere cap) of an exit head section of a shell-and-tube heat exchanger with two identical outlet-tubes that are symmetric with respect to the symmetry plane of the hemispherical exit head section of the heat exchanger. The volume flow rate through the tunnel is measured with a fluted tube (section 4). This fluted tube has an inner diameter of 50 mm and a length of 2 m, and is equipped with a multiport averaging Pitot tube [11] to measure flow rate. Calibration and use of such fluted tube for measuring flow rate were reported by Wang et al. [12]. The suction of a blower with variable speed electric motor (section 6) was used to control and adjust the air flow rate through the tunnel.

An enlarged schematic of the test section (a simplified model of the exit head section of a shell-and-tube heat exchanger with outlet-tubes) is shown in Fig. 2. It is half of a hemispherical cap mounted with two outlet-tubes and with a cylindrical inlet section at its opening. The vertical wall in the head section is used to separate the inlet flow from the outlet flow of the heat exchanger. The inlet flow enters the inlet head section of the heat exchanger in its way to the tubes that are in the shell of the heat exchanger. The exit flow from the tubes that are in the shell of the heat exchanger enter the exit head section on its way to the outlet tubes of the heat exchanger. The flow distribution in the exit head section and in the region of the outlet tubes is the subject of this study. Air enters this exit head section of the heat exchanger (the test section), converges into the outlet-tubes, passes through the collection section and the stabilization section where its volume flow rate is measured, and then exits through the diverging section and through the suction blower. Some of the dimensions for the test section are listed as follows, $R_s = 0.149$ m, $R_{in} = 0.145$ m, $l_s = 0.001$ m, $H = 0.200$ m, $H_1 = 0.043$ m, $L = 0.082$ m, and $d = 0.050$ m.

The velocity measurements were performed with dual-probe, six-beam, three-components, backward-scattering laser Doppler velocimeter (LDV). The front lens of the probes has a diameter of 50 mm, and a focal length of 350 mm. The angle between the two



1 - heat exchanger head section; 2 - outlet-tube; 3 - converging section; 4 - fluted tube;
5 - diverging section; 6 - blower; 7 - adjustable support

Fig. 1 Schematic of wind tunnel and test section

measuring probes of the LDV system was kept at 30 deg and the Doppler signals were transmitted through fiber optics to a burst spectrum analyzer. The seeding particles (having a mean diameter of less than $2 \mu\text{m}$) were generated by a six-jet atomizer, and glycerin was used as the seeding fluid. The laser beams from the LDV system enter from the inlet (x, y) plane of the test section (at $z=0.0 \text{ mm}$), and the measuring probe volume can be moved to locations inside the test section by the 3D (x, y, z) computer-controlled traversing system. The size of the probe volume was approximately $60 \mu\text{m}$ in length, and the resolution of the traverse system was 0.03 mm .

The LDV data acquisition system was operated continuously in the "coincidence" mode requiring simultaneous detection of samples in three coordinate directions, i.e., from the same scattering particle. If any of the six laser beams from the two probes is blocked by the solid walls of the test section, coincidence measurements could not be performed (data was not acquired for any of the velocity components). Therefore, at the inlet (x, y) plane of the test section ($z=0.0 \text{ mm}$), the measuring probe volume can be moved to almost any location on that intersecting plane. However, for (x, y) planes that are deeper in the test geometry and in the neighborhood of the outlet-tube (i.e. $z > 100 \text{ mm}$), a limited number of measurements could be made due to one or more of the laser beams being blocked by the solid wall of the test section. For

each point, data collection was programmed to acquire 64,000 samples or to measure for a duration of two minutes, whichever came first. Normally, the former criterion was satisfied except in the vicinity of the wall where particle arrival rates were reduced. The LDV software discarded data that was outside the range of $\pm 3\sigma$ from the mean value, and this filtering removed only the spurious data and not the valid turbulence data. The velocity bias correction technique used ensemble analysis as its basis, and applied a weighting function to each data point. The ensemble "corrected" values can be obtained through the number of data points and the weighting function. In the current software, the weighting function is determined using the time between data (TBD) points method [13]. In this method, the weighting function is the time between each realization or inter-arrival time. The LDV system was calibrated and the uncertainties for mean velocities were estimated to be less than $\pm 1.5\%$ with a typical inlet average velocity of 2.4 m/s . The results of many measurements at one point inside the flow field were checked at a fixed and steady flow rate and the measured mean velocity was repeatable with deviations of less than $\pm 0.6\%$ for the streamwise velocity component (v_z), and $\pm 1.5\%$ for the other two velocities components (v_x and v_y), respectively. Uncertainties of the experimental results were estimated by using the root-sum-square method [14]. From the calibration of the measuring instruments, the uncertainties of mea-

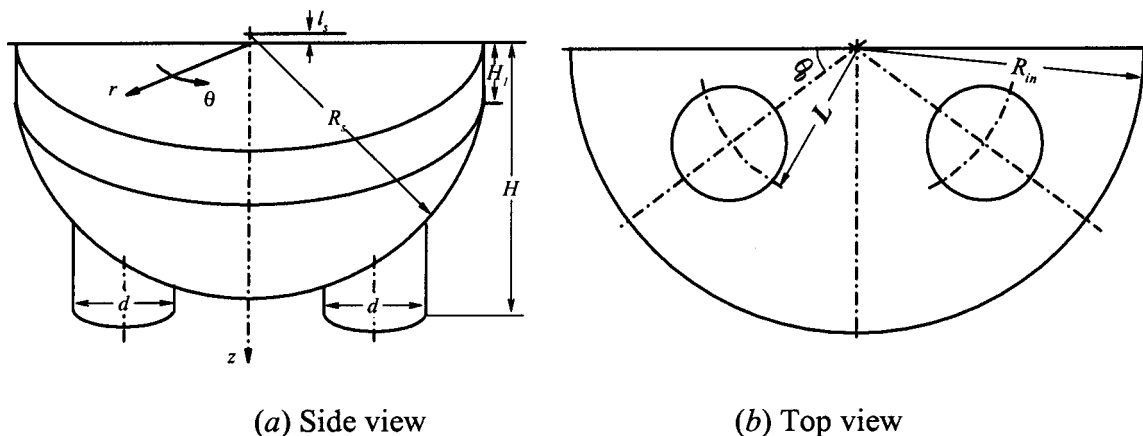


Fig. 2 Schematic for the exit head section of the heat exchanger

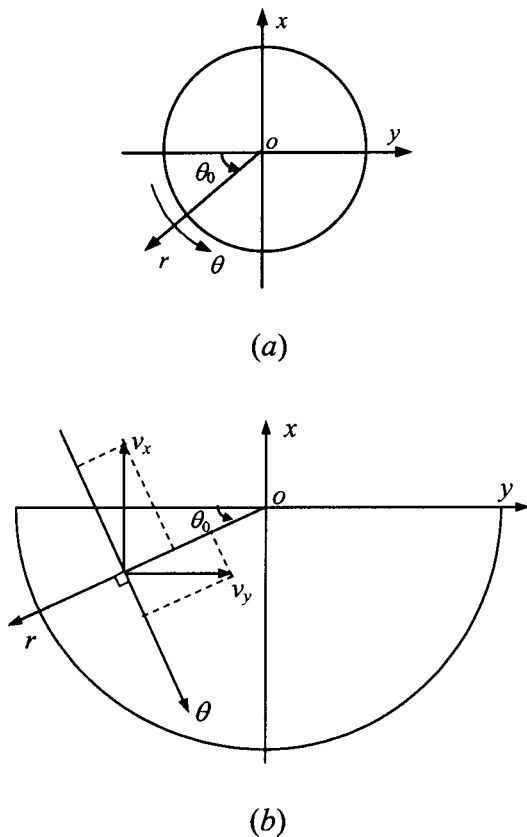


Fig. 3 Coordinates transformations for the traverse system and the measured velocities

measured values for Reynolds number (Re), and friction factor (f), were determined to be 5.6%, and 7.2%, respectively.

The traverse mechanism of the LDV system moved along the Cartesian coordinates (x, y, z), where (x, y) planes represents planes that are parallel to the inlet plane to the test section, and the z -coordinate represents the depth into the test section as shown in Figs. 2 and 3. The measured velocity components (v_x, v_y, v_z) in Cartesian coordinates (x, y, z) are transformed to velocity components (u, v, w) in cylindrical coordinates (r, θ, z), as shown in Fig. 3. It should be noted that the cylindrical coordinate will be used to display the measured fluid velocities and their fluctuations in the investigated cylindrical-hemispherical geometry. The transformation from the Cartesian coordinates system (x, y, z) that describes the movements of the traversing system, to the cylindrical coordinates (r, θ, z) that describes the cylindrical-hemispherical shape of the exit head section geometry of the heat exchanger (the test section), is shown in Fig. 3a for the specific case of $\theta = \theta_0$. Similarly, the measured velocity components (v_x, v_y, v_z) in Cartesian coordinates are transformed to the velocity components (u, v, w) in cylindrical coordinates for the specific case of $\theta = \theta_0$, by using Eq. (1) as shown in Fig. 3b:

$$\left. \begin{aligned} u &= -v_x \cos \theta_0 + v_y \sin \theta_0 \\ v &= -v_x \sin \theta_0 - v_y \cos \theta_0 \\ w &= v_z \end{aligned} \right\} \quad (1)$$

A photograph that shows the laser Doppler system and the inlet test section of the air tunnel (exit head section of the shell-and-tube heat exchanger with two outlet-tubes) is presented in Fig. 4.

Results and Discussions

Due to symmetry in the geometry of the test section, relative to the two outlet-tubes as shown in Fig. 2b, the measuring effort is simplified and reduced by restricting it to only one quarter of the

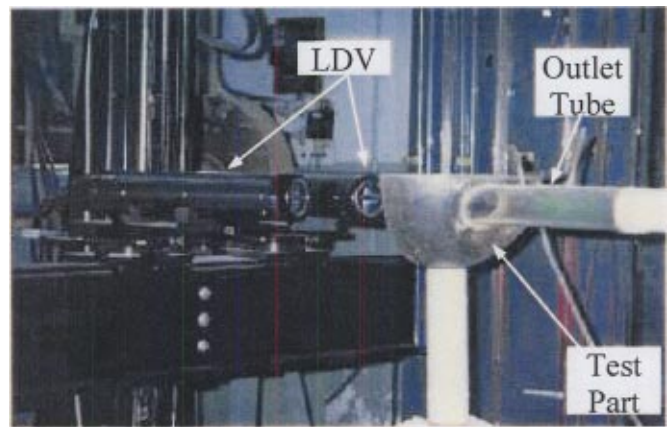
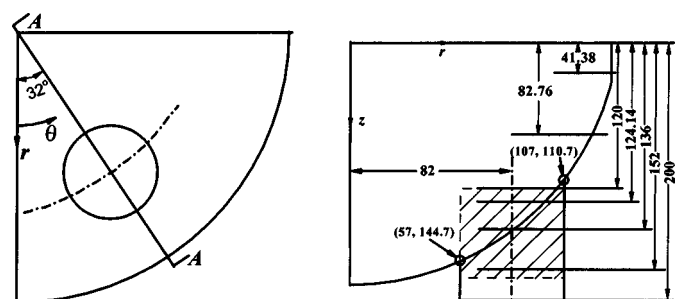


Fig. 4 Laser Doppler system and the test section

hemispherical cap. Laser Doppler velocity measurements were made only on the plane intersection of $\theta = 32$ deg with the test section (exit head section of the heat exchanger). This plane is in the radial and vertical directions (r, z) where the tangential coordinate is constant ($\theta = 32$ deg). It passes through both the center of the exit head section ($r = 0.0$ mm) and the center of the left outlet-tube ($r = 82$ mm and $\theta = 32$ deg) as shown schematically by a top view as Section A-A in Fig. 5a. A plane view of that intersecting plane (Section A-A in Fig. 5a) is shown in Fig. 5b, and as can be seen it cuts both the hemispherical head section of the heat exchanger and the outlet-tube. All the reported velocity measurements were made on this plane and it will be identified through the text as the measuring plane A-A. In the present study, the Reynolds number (Re) is defined as $Re = \rho w_{in} (2R_{in}) / \mu$, where w_{in} is the average streamwise velocity component at the inlet plane ($z = 0.0$ mm) of the test section, the density (ρ) and dynamic viscosity (μ) are taken as constant ($\rho = 1.24$ kg/m³ and $\mu = 1.83 \times 10^{-5}$ kg/m·s). The average inlet air velocity is determined through the expression of $w_{in} = Q / A_{in}$, where Q is the air volumetric flow rate measured by the fluted-tube (section 4 as shown in Fig. 1), and A_{in} is the cross-sectional flow area at the inlet plane of the test section.

The mean and turbulent fluctuating velocity components were measured in the test section on the selected measuring plane A-A, and the measurements of the mean velocity components are reported in Figs. 6 and 7 for Reynolds number of $Re = 46122$. The results in Fig. 6 represent a vector plot of the mean velocity on the measuring plane A-A, and they clearly show how the flow converges to the outlet-tube while velocity vectors change directions and magnitudes due to changes in geometry. The velocity at the inlet of the measuring plane A-A ($z = 0.0$ mm) is relatively small and uniform, while the velocity at the inlet of the outlet-tube in



(a) Top view

(b) A-A intersection

Fig. 5 Planes where measurements are made

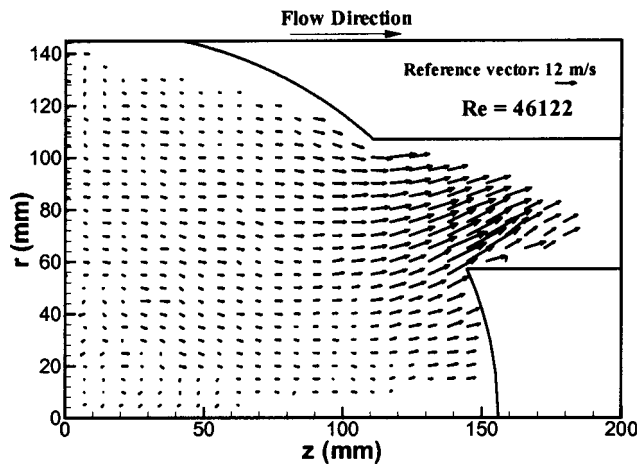
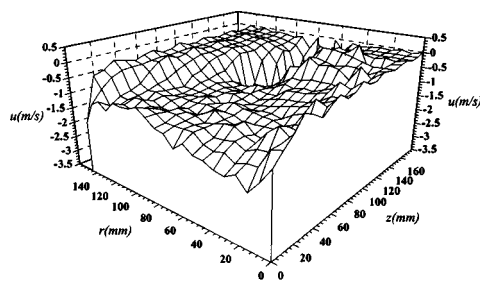
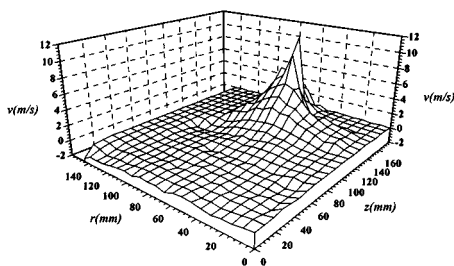


Fig. 6 Velocity vector field on the measuring plane A-A for $Re=46,122$

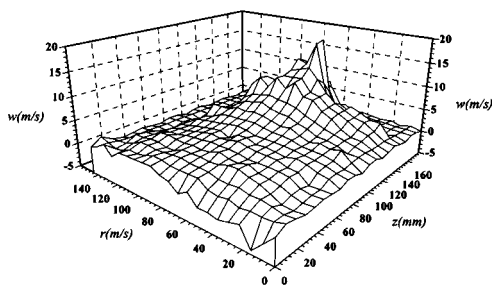
the measuring plane A-A is relatively high and nonuniform. The radial velocity component (v) is of the same order of magnitude as the streamwise velocity component (w) in the neighboring region of the outlet-tube on the measuring plane A-A. The streamwise velocity component (w) increases and the radial velocity



(a) Contours of velocity component (u)



(b) Contours of radial velocity component (v)



(c) Contours of streamwise velocity component (w)

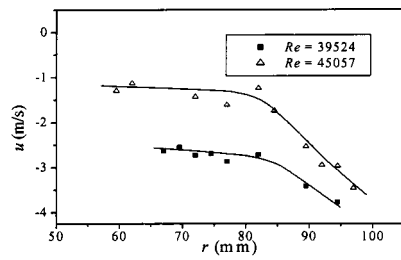
Fig. 7 Distribution of velocity components on the measuring plane A-A for $Re=46,122$

component (v) decreases gradually as the flow enters the outlet-tube on the measuring plane A-A.

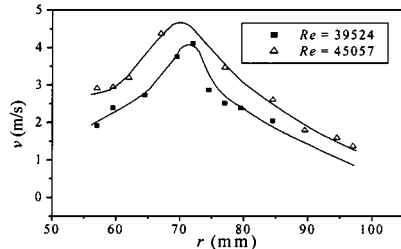
Distributions of the measured three velocity components on the measuring plane A-A are presented in Fig. 7 for $Re=46122$. It can be seen from Fig. 7(a) that tangential velocity component (u) is small in the whole region of that plane, ranging between -2 to 0.5 m/s and the negative sign means that the velocity is in the reverse θ -direction as denoted in Fig. 3. It is negative on most of that plane, which means that fluid below the measuring plane A-A (i.e., $\theta < 32$ deg) rotates in a clockwise direction (as viewed along z axis direction) while fluid that is above the measuring plane A-A ($\theta > 32$ deg) rotates in a counterclockwise direction. This is due to the fact that the centerline of the outlet-tube is not symmetric relative to tangential direction in the test section, i.e. the centerline of the outlet-tube is at 58 deg from the top half of the test section and at 32 deg from the bottom half as shown in Fig. 5(a). The larger flow area that exists above the the $\theta=32$ deg plane is responsible for making the average tangential velocity component (u) negative on most of this plane. The results in Fig. 7(b) show that the radial velocity component (v) on the measuring plane A-A increases sharply close to the inlet of the outlet-tube due to the abrupt decrease in flow cross sectional area. That velocity component (v) is positive throughout that plane because fluid flows from the larger area at the inlet of that plane ($z=0.0$ mm) toward the smaller area of outlet-tube as shown in Fig. 6. The results in Fig. 7(c) show that the streamwise velocity component (w) on the measuring plane A-A increases gradually from the inlet of that plane to the inlet of the outlet-tube on that plane. On the measuring plane A-A, the maximum of this velocity component occurs at the center of the outlet-tube and its magnitude decreases gradually to zero at the wall of the outlet-tube. These results clearly show that the position of the outlet-tube influences significantly the velocity distribution in the exit head section of the shell and tube heat exchanger. Decreasing the nonsymmetry of the outlet-tube could help in decreasing nonuniformity in the velocity distribution.

The previous results demonstrate that most of the variations in the velocity field on the measuring plane A-A occur in the region where the outlet-tube intersects with the hemispherical exit head section of the heat exchanger. The region of $120 \leq z \leq 160$ mm and $57 \leq r \leq 107$ mm on the measuring plane A-A (the dashed area in Fig. 5(b)) is investigated in more details in order to quantify the velocity field in that region. The radial distributions of the three mean velocity components on three “ z ” planes at the entrance region of the outlet-tube ($z=120, 136$ and 152 mm) on the measuring plane A-A are shown in Figs. 8, 9 and 10. The solid lines that are shown in these figures represent a best fit to the measured results. The streamwise intersection of $z=120$ mm lies at the beginning of the region where the outlet-tube intersects with the hemispherical exit head section of the heat exchanger. The streamwise intersection of $z=136$ mm lies in the middle of that region, and the streamwise intersection of $z=152$ mm lies at the end of that region as shown schematically in Fig. 5(b).

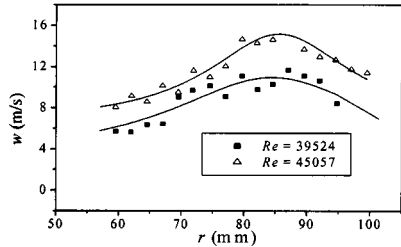
The results in Fig. 8 show the radial distributions of the three mean velocity components on the measuring plane A-A at $z=120$ mm for Reynolds numbers of $39,524$ and $45,057$. The tangential velocity component (u) on that plane is negative on this z -line and is relatively uniform until the centerline of the outlet-tube ($r=82$ mm). Its negative magnitude starts to increase sharply as the radial distance (r) continues to increase. The radial velocity component (v) shows a peak value of about 4.5 m/s for Reynolds number of 45057 at $r \approx 73$ mm (a distance smaller than the centerline location of the outlet-tube that is at $r=82$ mm), then decreases as the distance approaches the solid wall boundary of the test section. The streamwise velocity component (w) shows a peak of 15 m/s for Reynolds number of 45057 at approximately $r=82$ mm (the location of the centerline of the outlet-tube), then its magnitude decreases as the distance approaches the solid wall



(a) Tangential velocity component (u)



(b) Radial velocity component (v)

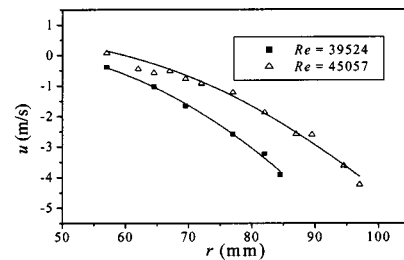


(c) Streamwise velocity component (w)

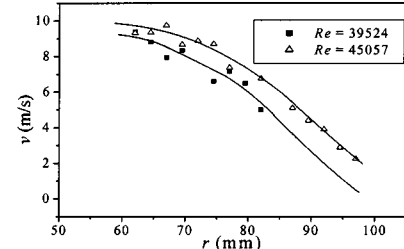
Fig. 8 Velocity distributions on the measuring plane A-A at $z=120$ mm

boundary of the outlet tube. All of these three velocity components (u , v and w) increase in magnitude with the increasing Reynolds number, but they retain approximately the same general distribution. Similar trends in the results can be seen in Fig. 9 for $z=136$ mm on the measuring plane A-A, with the exceptions that the peaks that were observed in two of these velocity distributions in Fig. 8 (for $z=120$ mm) do not appear at this z location. The results presented in Fig. 10 for $z=152$ mm on the measuring plane A-A show similar trends but with peaks in the distributions at roughly $r=65$ mm (a distance smaller than the centerline location of the outlet-tube). It should be noted that the maximum tangential velocity component (u) at $z=152$ mm, is positive and lies in the region of $r=60\sim 65$ mm. That velocity component experiences significant variation in its magnitude and direction in this region as the fluid enters the outlet-tube. Baffles or similar structures could be installed in the exit head section of the heat exchanger to improve the quality of the flow in the outlet-tubes.

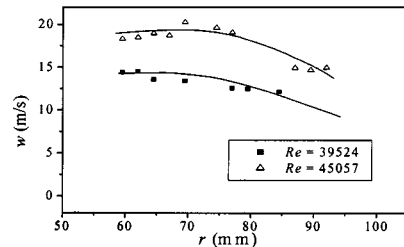
Radial distributions of the three mean velocity components on the measuring plane A-A are presented in Fig. 11 for three z -locations ($z=41.38$ mm, 82.76 mm and 124.14 mm) for $Re=46122$. The line of $z=41.38$ mm lies in the cylindrical section of the exit head section of the heat exchanger. The line of $z=82.76$ mm lies in the hemispherical region, and the line of $z=124.14$ mm lies in the region where the outlet-tube intersects with the hemispherical cap of the exit head section as shown in Fig. 5b. The outer solid wall boundary of the test section at these z -locations are at $r=145$ mm, 125.64 mm, and 107 mm, respectively. Distributions of the three mean velocity components at $z=41.38$ mm and $z=82.76$ mm are similar in nature since these



(a) Tangential velocity component (u)



(b) Radial velocity component (v)

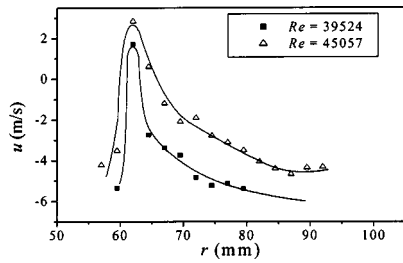


(c) Streamwise velocity component (w)

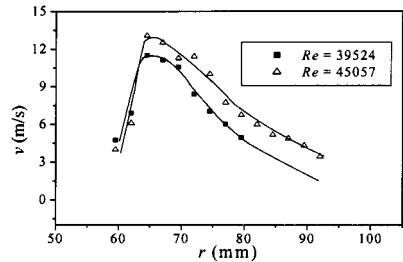
Fig. 9 Velocity distributions on the measuring plane A-A at $z=136$ mm

two locations have similar geometries but differ in size. On these two z -lines, the tangential velocity component (u) and the radial velocity component (v) are relatively low, and the streamwise velocity component (w) increases as the flow cross sectional area decreases from that at $z=41.38$ mm to that at $z=82.76$ mm. The streamwise velocity component on the measuring plane A-A at these two locations develops a positive peak value at approximately $r=85$ mm (a distance approximately equal to the centerline location of the outlet-tube). The further decrease in the cross sectional area at the streamwise location of $z=124.14$ mm causes the fluid to accelerate and converge toward the outlet-tube with a maximum tangential velocity component (u) of -3 m/s developing at $r\approx 90$ mm. That velocity component is relatively small but positive in the region between $r=20$ to 50 mm, and it is negative for larger radial distances, implying a vortical clockwise type flow into the outlet-tube at this z -plane. Similar conclusion could be drawn from the results that are presented in Fig. 10a. The radial velocity component (v) reaches a maximum of about 5 m/s, and the streamwise velocity component (w) reaches a maximum of about 16 m/s at $r\approx 70$ mm. The streamwise velocity component experiences the greatest change due to the greatest change in the cross sectional area. Its maximum of about 16 m/s that occurs at $z=124.14$ mm is about four times the maximum that occurs at $z=41.38$ mm.

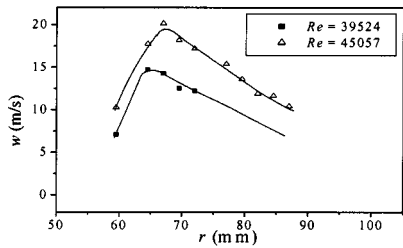
Radial distributions of the Reynolds normal stresses ($\overline{u'u'}$, $\overline{v'v'}$ and $\overline{w'w'}$) on the measuring plane A-A at three selected streamwise locations ($z=41.38$, 82.76 and 124.14 mm) are shown in Fig. 12 for $Re=46122$. The interference of the solid wall boundaries of the test section with the laser beams of the LDV



(a) Tangential velocity component (u)

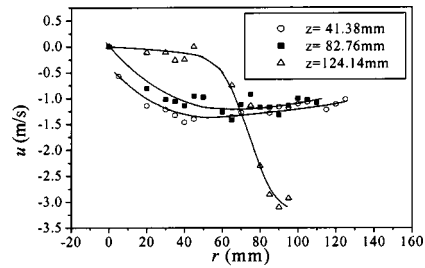


(b) Radial velocity component (v)

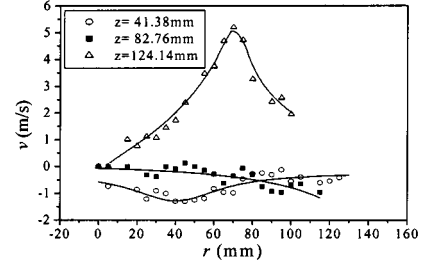


(c) Streamwise velocity component (w)

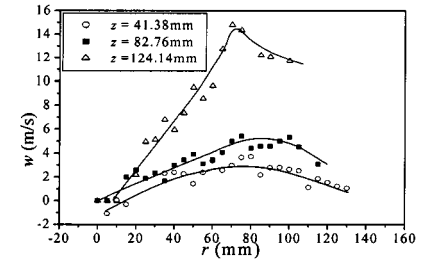
Fig. 10 Velocity distributions on the measuring plane A-A at $z=152$ mm



(a) Tangential velocity component (u)



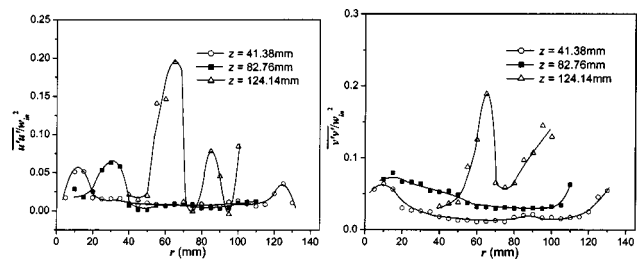
(b) Radial velocity component (v)



(c) Streamwise velocity component (w)

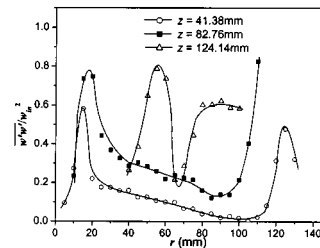
Fig. 11 Radial distribution of mean velocity components on the measuring plane A-A for $Re=46,122$

system at $z=82.76$ and 124.14 mm limits the number of data points that can be taken on these locations as can be seen from Figs. 11–13. The Reynolds stresses are normalized based on the inlet average streamwise velocity component (w_{in}), which is 2.347 m/s for $Re=46122$. The solid lines that appear in these figures are an attempt to connect the experimental points while smoothing the transition from one point to the other. Figure 12(a) shows that the tangential Reynolds normal stress component, $u'u'$, is relatively low on the measuring plane A-A in the whole radial direction at $z=41.38$ and 82.76 mm. At $z=124.14$ mm, a peak appears to develop at $r \approx 65$ mm (near the inner solid wall of the outlet tube that is at $r=57$ mm), and a minimum value appears to develop at $r \approx 75$ mm (near the centerline of the outlet tube that is at $r=82$ mm). The points that appear in the figure on a $z=124.14$ mm and $r > 82$ mm are below the original hemispherical surface shape of the test section, and are inside the domain of the outlet tube. The tangential velocity component is negative in that region, and the wall of the outlet-tube starts to influence significantly the behavior on the tangential Reynolds normal stress component in that region. Figure 12(b) shows that the radial Reynolds normal stress component ($v'v'$) is also low on the measuring plane A-A in the whole radial range at $z=41.38$ and 82.76 mm. At $z=124.14$ mm, one peak develops at about $r \approx 65$ mm (close to the inner solid wall of the outlet-tube), and that is in the same general location where the peak tangential Reynolds normal stress component ($u'u'$) develops, as seen in Fig. 12(a). Another peak appears to develop on this z -location at $r \approx 100$ mm (close to the outer solid wall of the outlet-tube that is at $r=107$ mm). Fig.



(a)

(b)



(c)

Fig. 12 Radial distribution of Reynolds normal stress components on the measuring plane A-A for $Re=46,122$

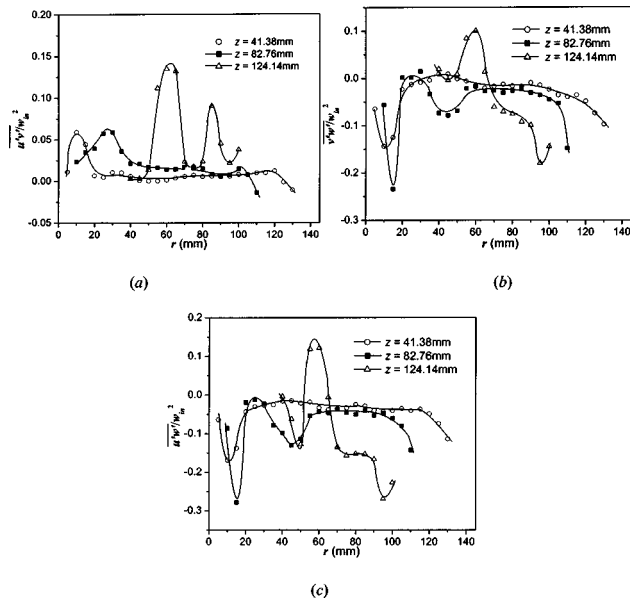


Fig. 13 Radial distribution of Reynolds shear stress components on the measuring plane A-A for $Re=46,122$

Figure 12(c) shows that the peak values in the distributions of the streamwise Reynolds normal stress component ($w'w'$) also develop in the same general regions on $z=124.14$ mm. The maximum value of the streamwise Reynolds normal stress component ($w'w'$) is about four times higher than the maximum values of the tangential and the radial Reynolds normal stress components. The peaks that develop in Fig. 12(c) at $z=41.38$ mm and 82.76 mm are due to the proximity of these locations to the solid boundary and symmetry line of the hemispherical test section. The solid wall boundary of the test section at these z -locations are at $r=145$ and 125.64 mm, respectively. Radial distributions of the Reynolds shear stress components ($u'v'$, $v'w'$ and $u'w'$) on the measuring plane A-A at three streamwise locations ($z=41.38$, 82.76 and 124.14 mm) are presented in Fig. 13 for $Re=46,122$. The results for the Reynolds shear stress components are normalized based on the average inlet velocity ($w_{in}=2.347$ m/s for $Re=46,122$). The Reynolds shear stress component, $u'v'$, is relatively low at $z=41.38$ and 82.76 mm. All three shear stress components at $z=124.14$ mm have a positive peak value in the same general radial location of about $r\approx 60$ mm, similar to what was observed for the Reynolds normal stress components on the same z -location as can be seen in Fig. 12. Both $v'w'$ and $u'w'$ are negative over most of the radial range for $z=41.38$ mm, and 82.76 mm, while at $z=124.14$ mm they exhibit both positive and negative peaks.

Radial distributions of the Reynolds normal stress components ($u'u'$, $v'v'$ and $w'w'$) on the measuring plane A-A are presented in Fig. 14 for three z -locations that are in the neighborhood of the outlet-tube ($z=117.24$, 137.93 and 151.72 mm). The interference of the solid wall boundaries of the test section with the laser beams of the LDV system at these locations, limits the number of measuring data points that can be taken as can be seen from Figs. 14 and 15. Very limited number of measurements could be made at $z=151.72$ mm. The Reynolds normal stress components, $u'u'$ and $v'v'$, are relatively low in most of the radial range at $z=117.24$ mm. All three Reynolds normal stress components develop a peak at $r\approx 60$ mm (near the inner solid wall of the outlet tube) at $z=137.93$ mm. The magnitudes of the Reynolds normal stress components at these z -locations (in the neighborhood of the outlet-tube) are higher than those presented in Fig. 12. One of the common features in the radial distributions of the Reynolds normal

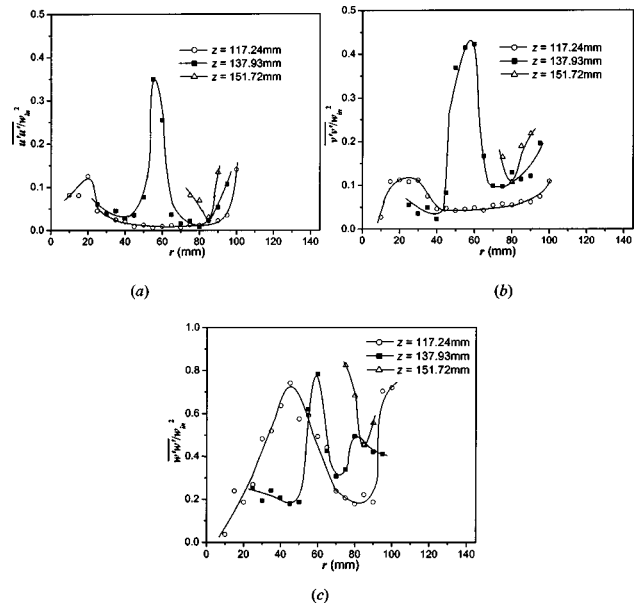


Fig. 14 Radial distribution of Reynolds normal stress components on the measuring plane A-A in the inlet region of the outlet-tube for $Re=46,122$

stress components is that they all exhibit a lower value in the region near the centerline of the outlet-tube ($r=82$ mm) at these z -locations. Radial distributions of the Reynolds shear stress components ($u'v'$, $v'w'$ and $u'w'$) on the measuring plane A-A are presented in Fig. 15 for the same z -locations as the ones presented in Fig. 14 ($z=117.24$, 137.93 and 151.72 mm). The results that are presented for $z=137.93$ mm, exhibit a positive peak in the distribution of the Reynolds shear stress $u'v'$ component, and negative peaks in the distributions of the other two Reynolds shear stress components $v'w'$ and $u'w'$ at $r\approx 60$ mm (close to the inner wall of the outlet tube). This roughly the same region where all the three Reynolds normal stress components exhibit a maximum

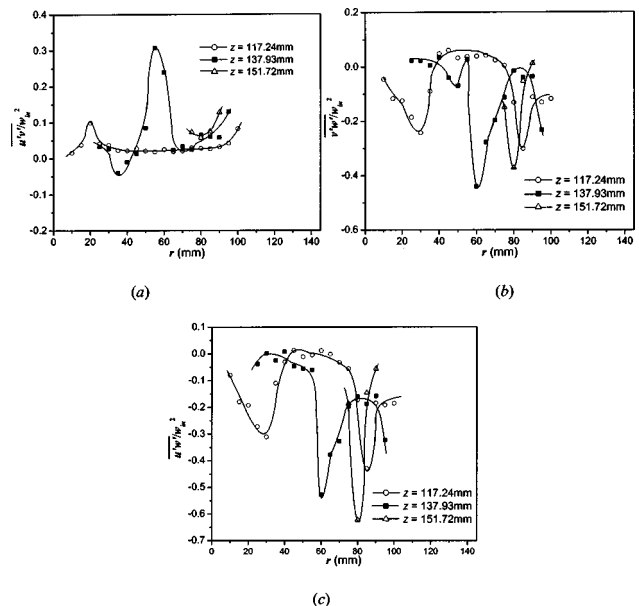


Fig. 15 Radial distribution of Reynolds shear stress components on the measuring plane A-A in the inlet region of the outlet-tube for $Re=46,122$

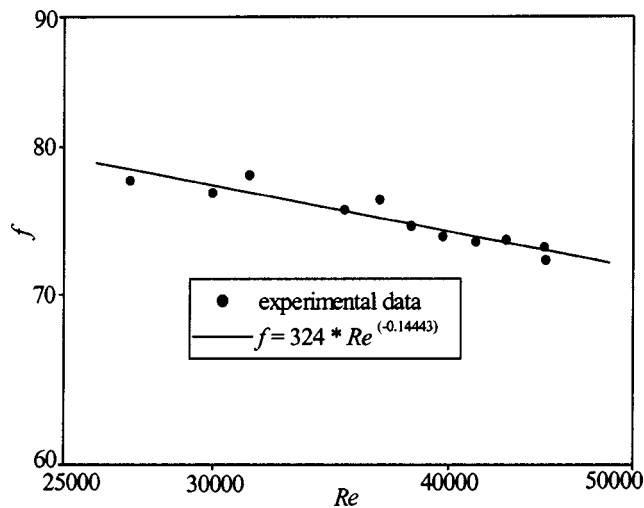


Fig. 16 Variation of the friction factor as a function of Reynolds numbers

at the same z -location, as can be seen in Fig. 14. The magnitudes of the Reynolds shear stress components on these z -locations (in the neighborhood of the outlet-tube) are generally higher than the one presented in Fig. 13. The pressure drop across the exit head section and the outlet-tube, and the flow rate, were measured and used to calculate the friction factor as a function of Reynolds number. The friction factor is defined as:

$$f = (p_{in} - p_{out} + 0.5\rho w_{in}^2 - 0.5\rho w_{out}^2) / (0.5\rho w_{in}^2) \quad (2)$$

where p_{in} and p_{out} are static pressures at the inlet and outlet sections respectively, and w_{out} is the mean velocity in the streamwise direction along the outlet-tube (the outlet-tube diameter $d_{out} = 0.05$ m). The inlet pressure p_{in} is taken as the atmospheric pressure and the outlet pressure p_{out} is measured through the pressure tap on the wall of the outlet-tube at $z = 200$ mm. The results that are presented in Fig. 16 show that the friction factor decreases as the Reynolds number increases in the experimental range, and its behavior can be described by the relation of $f = 324 Re^{-0.14443}$.

Conclusions

Measurements of the three mean velocity components and the Reynolds stress components are reported for three-dimensional turbulent flow in a model for the exit head section of a shell-and-tube heat exchanger with outlet-tubes. Measurements of velocities in the test section are presented for only one intersecting θ -plane ($\theta = 32$ deg) as a function of r and z . The results show that the flow in that measuring plane A-A is nonuniform and complex in the region where the outlet-tubes are connected to the exit head section of the heat exchanger. The fluid converges into the outlet-tube with vortical motion and in that region the velocity components in the radial and streamwise directions are of the same order of magnitude. The velocity distribution in that region is not symmetric in either tangential or radial directions, because the outlet-tubes are not symmetrically located relative to these two directions. The tangential Reynolds normal stress component is relatively low in the whole radial range at $z = 41.38$ and 82.76 mm. At $z = 124.14$ mm, all of the Reynolds stress components (normal and shear) exhibit a peak at approximately $r = 60$ mm (close to the inner solid wall of the outlet-tube). The results that are presented for $z = 137.93$ mm, exhibit a positive peak in the distribution of the Reynolds shear stress $\overline{u'v'}$ component, and negative peaks in the distributions of the other two Reynolds shear stress components $\overline{v'w'}$ and $\overline{u'w'}$ at $r \approx 60$ mm (close to the inner solid wall of the outlet-tube). This is roughly the same region

where all the three Reynolds normal stress components exhibit a maximum at the same z -location. The magnitudes of the Reynolds normal and shear stress components in the neighborhood of the outlet-tube $z > 124.14$ mm are higher than those measured in the hemispherical portion of the test section at $z < 124.14$ mm. The measured friction factor decreases as the inlet Reynolds number increases from 27,097 to 45,010.

Acknowledgments

This work was supported in part by grants from the National Science Foundation of China (NNSFC) (No. 59676019), the Research Fund for the Doctoral Program of Higher Education (RFDP) (No. 9589801), and the US Department of Energy Grant No. DE-FG02-03ER46067.

Nomenclature

- A_{in} = inlet cross sectional area of the head section of the heat exchanger
- d = inner diameter of the outlet-tube
- f = friction factor
- p = pressure
- Q = volume flow rate
- r = radial direction (in cylindrical coordinates)
- R_{in} = inlet radius of the heat exchanger head section
- R_s = spherical radius of the heat exchanger head section
- Re = Reynolds number = $\rho w_{in}(2R_{in})/\mu$
- u = velocity component in the θ -direction (in cylindrical coordinates)
- $\overline{u'u'}$ = Reynolds normal stress component
- $\overline{u'v'}$ = Reynolds shear stress component
- $\overline{u'w'}$ = Reynolds shear stress component
- v = velocity component in the r -direction (in cylindrical coordinates)
- $\overline{v'v'}$ = Reynolds normal stress component
- $\overline{v'w'}$ = Reynolds shear stress component
- v_x = velocity component in the x -direction (in Cartesian coordinates)
- v_y = velocity component in the y -direction (in Cartesian coordinates)
- v_z = velocity component in the z -direction (in Cartesian coordinates)
- w = velocity component in the z -direction (in cylindrical coordinates)
- w_{in} = average inlet streamwise velocity component
- $\overline{w_{out}}$ = average outlet streamwise velocity component
- $\overline{w'w'}$ = Reynolds normal stress component
- x, y, z = directions of Cartesian coordinates

Greek Symbols

- μ = dynamic viscosity
- ρ = density
- θ = circumferential direction (in cylindrical coordinates)

References

- [1] Christolm, D., 1980, *Developments in Heat Exchanger Technology—I*, Applied Science Publishers, London, England.
- [2] Huppert, T., 2000, *Heat Exchanger Design Handbook*, Marcel Dekker, New York.
- [3] Shah, R. K., and London, A. L., 1978, *Laminar Flow Forced Convection in Ducts*, Academic Press, New York.
- [4] Kakac, S., and Liu, H. T., 1997, *Heat Exchangers: Selection, Rating, and Thermal Design*, CRC Press, New York.
- [5] Bremhorst, K., and Flint, P. J., 1991, "The Effect of Flow Patterns on the Erosion/Corrosion of Shell and Tube Heat Exchangers," *Wear*, **145**, pp. 123–135.
- [6] Yu, B., Nie, J. H., Wang, Q. W., and Tao, W. Q., 1999, "Experimental Study on the Pressure Drop and Heat Transfer Characteristics of Tubes with Internal Wave-Like Longitudinal Fins," *Heat Mass Transfer*, **35**, pp. 65–73.

- [7] Halle, H., Chenoweth, J. M., and Wambsganss, M. W., 1984, "Shell Side Water Flow Pressure Drop Distribution Measurements in an Industrial-Sized Test Heat Exchanger," In: A Reappraisal of Shell Side Tube Flow in Heat Exchangers," 22nd Heat Transfer Conference and Exhibition, Niagara Falls, ASME, HTD **36**, pp. 37–48.
- [8] Zhang, C., 1994, "Numerical Modeling Using a Quasi-Three-Dimensional Procedure for Large Power Plant Condensers," ASME J. Heat Transfer, **116**, pp. 180–188.
- [9] Prithiraj, M., and Andrews, M. J., 1998, "Three Dimensional Numerical Simulation of Shell-and-Tube Heat Exchangers—Part I: Foundation and Fluid Mechanics," Numer. Heat Transfer, Part A, **33**, 799–816.
- [10] Tao, W. Q., Nie, J. H., Cheng, P., and Wang, Q. W., 2001, "Numerical Simulation of Three-Dimensional Turbulent Flow in a Complex Geometry, with LDV Experimental Confirmation," Proceedings of 2nd ICHMT Symposium on Advances in Computational Heat Transfer, Queensland, Australia, pp. 1235–1242.
- [11] Miller, R. W., 1996, *Flow Measurement Engineering Handbook*, 3rd ed., McGraw-Hill, New York.
- [12] Wang, L. B., Tao, W. Q., Wang, Q. W., and He, Y. L., 2001, "Experimental and Numerical Study of Turbulent Heat Transfer in Twisted Square Ducts," ASME J. Heat Transfer, **123**, pp. 868–877.
- [13] Barnett, D. O., and Bentley, H. T., 1974, "Statistical Bias of Individual Realization Laser Velocimeters," Proceedings of the Second International Workshop on Laser Velocimetry, Engineering Extension Series, Purdue University, **144**, pp. 428–444.
- [14] Moffat, R. J., 1988, "Describing the Uncertainties in Experimental Results," Exp. Therm. Fluid Sci., **1**, pp. 3–17.